Cardiovascular Revascularization Medicine 20 (2019) 858–864

Contents lists available at ScienceDirect

Cardiovascular Revascularization Medicine

Resorbable Magnesium Scaffold in Coronary Bifurcations – Report of in Vitro Experiments☆

Gabor G Toth [a,b], Michael Haude [c], Daniel Lootz [d], Mariano Pellicano [b,e], William Wijns [f,*]

[a] University Heart Centre Graz, Medical University of Graz, Austria
[b] Cardiovascular Research Centre Aalst, OLV-Clinic Aalst, Belgium
[c] Medical Clinic I, Städtische Kliniken Neuss, Lukaskrankenhaus GmbH, Germany
[d] Biotronik AG, Bülach, Switzerland
[e] Department of Advanced Biomedical Sciences, Federico II University of Naples, Naples, Italy
[f] The Lambe Institute for Translational Medicine and Curam, National University of Ireland, Galway, Ireland

ARTICLE INFO

Article history:
Received 29 October 2018
Received in revised form 27 November 2018
Accepted 27 November 2018

Keywords:
Resorbable magnesium scaffold
Coronary bifurcation
In vitro

ABSTRACT

Objectives: The aim of this work is to evaluate in an in vitro setting the behavior of resorbable magnesium scaffolds (RMS) in bifurcations.
Background: As coronary bifurcations represent an important portion of all PCIs, it is crucial to understand whether RMS is applicable in these complex lesions.
Methods: Performance of RMS was evaluated with focus on bifurcations. In bifurcations RMS was tested for (1) main branch stenting with side branch opening and proximal optimization; for (2) main branch stenting with final kissing and proximal optimization; for (3) T-and-protrusion technique; for (4) string technique, which is a minimalistic version of conventional culotte technique. All tests were performed using 3.50 × 25 mm RMS. Results were evaluated by fluoroscopy, optical coherence tomography (OCT) and micro-computed tomography (μCT), for scaffold conformability, strut apposition, structural deformation and strut fracture.
Results: All planned procedural steps were performed successfully with good result according to fluoroscopy. By OCT the overall malapposition rate in bifurcation cases was 4.3%, occurring predominantly in the carinal area. No malapposition was seen at the proximal main branch confirming proper conformability of RMS. μCT analysis has shown that final kissing dilation resulted in fully stretched struts in cases, where performed with 3.5 and 3.0 mm balloons. In one case a broken connector (T-and-protrusion) and in another case, a broken strut (String technique) were identified.
Conclusions: RMS can structurally cope with bifurcations. Still, for cases and techniques where overexpansion beyond the recommended limit is needed, RMS might not be the proper device due to risk of strut fracture.

1. Introduction

Percutaneous coronary intervention (PCI) has shown continuous development since its introduction. First, metallic stents revolutionized our therapeutic approach compared to plain old balloon angioplasty and later the introduction of drug-eluting devices marked a new era in the fight against restenosis. Lately the establishment of a new frontier was anticipated from bioresorbable scaffolds, manufactured first of poly-L-lactic acid and more recently of magnesium. The pioneering concept of bioresorbable scaffolds offers proper vascular scaffolding in the short term, and the possibility of restoring physiologic vasomotion after resorption in the longer-term.

It must be acknowledged that the structural attributions of these devices are markedly different from currently available metallic stents in many respects: struts are not only almost twice as thick but also less flexible and more fragile, requiring careful handling. Therefore, before their clinical application in practice becomes possible, there is a definite need for evaluating their performance in various anatomical and clinical settings, where drug-eluting metallic stents are being used routinely with excellent short- and long-term outcomes.

As coronary bifurcations represent 10–15% of all PCIs [1], it is crucial to understand whether and to what extent bioresorbable scaffolds are applicable in these rather common complex lesions. Due to marked

Abbreviations: OCT, optical coherence tomography; PCI, percutaneous coronary intervention; POT, proximal optimization; RMS, resorbable magnesium scaffold; μCT, micro computed tomography.

☆ Conflicts of interest: GGT receives institutional research grant and honoraria for lecture from Biotronik, Abbott and Medtronic. MH receives honoraria for lecture from Biotronik. WW receives institutional research grant and honoraria for lecture from Biotronik, Micell and MicroPort. DL is Biotronik employee. MP has no conflicts of interest.

* Corresponding author.
E-mail address: william.wyns@gmail.com (W. Wijns).

https://doi.org/10.1016/j.carrev.2018.11.023
1553-8389/

variability in terms of distribution of atherosclerosic plaque, in terms of main branch and side branch calibers and in terms of their angulation, there is necessarily a significant discrepancy between the pure tubular shape of a stent and individual bifurcation anatomy. All currently widely accepted single- and double-stent techniques aim to address these variations, sometimes requiring a massive deformation of the original strut structure. While the behavior and performance of conventional metallic stents have been thoroughly investigated in vitro, as well as in vivo, our knowledge is still limited about bioresorbable vascular scaffolds, especially new technologies such as the resorbable magnesium scaffold (RMS) (Magmaris; Biotronik AG, Bülach, Switzerland).

The aim of the present work is to evaluate extensively in an in vitro setting the behavior of RMS in various non-bifurcation and bifurcation anatomies using standard interventional techniques.

2. Methods

Performance of RMS was evaluated in vitro with focus on bifurcations, as described in detail below. All the tests were performed using 3.50 × 25 mm RMS in 3D printed, pure saline-filled silicone vessel phantoms. 3D bifurcation models were produced by a polyjet printer, using rubber-like, elastomeric material, called TangoPlus™ (Sirris Inc., Brussels, Belgium). Procedures were performed under conventional fluoroscopic guidance. Results were evaluated by (1) fluoroscopy, (2) optical coherence tomography (OCT) and (3) micro-computed tomography (μCT), in terms of scaffold conformability, strut apposition, structural deformation and strut fracture, as detailed below. Procedural performance (i.e. cross-ability of a guidewire or a balloon to the side branch) was evaluated subjectively by the operator.

2.1. Steps of investigated procedures

The aim was to evaluate the performance of RMS in bifurcations, consistent with standardized techniques for clinical procedures [2]. Procedures were performed in two types of uniform silicone bifurcation models, where proximal main branch, distal main branch and side branch were 3.50/3.00/2.50 mm in diameter (*Model #1*), and 4.00 mm/3.50 mm/3.00 mm in diameter (*Model #2*), respectively. Angulation between distal main branch and side branch was uniformly 60°.

Procedures were performed in five different standardized ways, as detailed below [2]. *Model #1* was used for *Tests #1* and *#2* and *Model #2* was used for *Tests #3*, *#4* and *#5*, as specified below.

Test #1: Main branch scaffolding with side branch opening alone – small side branch*:* (1) First, the RMS was deployed in the main branch at 12 atm. (2) Second, proximal optimization (POT) was performed with a 3.50 mm non-compliant balloon (18 atm). (3) Then the side branch was wired with a regular workhorse guidewire through the most distal cell of the main branch scaffold, facing the side branch ostium. (4) A 2.50 mm balloon was positioned through the proximal main-branch to side branch continuum and inflated with 9 atm. (5) Finally, POT was repeated with a 3.50 mm non-compliant balloon, inflated to 18 atm to ensure good strut apposition (POT-side-POT approach).

Test #2: Main branch scaffolding with final kissing dilation – small side branch*:* (1) First, the RMS was deployed in the main branch with 12 atm. (2) Second, POT was performed with a 3.50 mm non-compliant balloon (18 atm). (3) Then the side branch was wired with a regular workhorse guidewire through the most distal cell of the main branch scaffold, facing the side branch ostium. (4) For final kissing dilation a 3.00 mm balloon was positioned into the main branch, while a 2.50 mm balloon was positioned in the side branch with minimal protrusion into the main branch ('snuggle fashion'). Balloons were inflated in sequential fashion, with 14 and 7 atm, respectively, starting with the side-branch balloon. (5) Finally, POT was repeated with a 3.50 mm non-compliant balloon, inflated to 18 atm.

Test #3: Main branch scaffolding with final kissing dilation – large side branch*:* (1) First, the RMS was deployed in the main branch with 12 atm. (2) Second, POT was performed with a 4.00 mm non-compliant balloon (18 atm). (3) Then the side branch was wired with a regular workhorse guidewire through the most distal cell of the main branch scaffold, facing the side branch ostium. (4) For final kissing dilation a 3.50 mm balloon was positioned into the main branch, while a 3.00 mm balloon was positioned in the side branch with minimal protrusion into the main branch ('snuggle fashion'). Balloons were inflated in sequential fashion, with 14 and 12 atm, respectively, starting with the side-branch balloon. (5) Finally, POT was repeated with a 4.00 mm non-compliant balloon, inflated to 18 atm.

Test #4: T and protrusion technique – large side branch*:* Procedure was performed as described in literature [3]. (1) First, the RMS was deployed in the main branch with 12 atm. (2) Second, POT was performed with a 4.00 mm non-compliant balloon (18 atm). (3) Then the side branch was wired with a regular workhorse guidewire through the most distal cell of the main branch scaffold, facing the side branch ostium. (4) Kissing dilation with a 3.50 mm balloon was positioned into the main branch, while a 3.00 mm balloon was positioned in the side branch with few millimeters of protrusion into the main branch. Balloons were inflated in sequential fashion, with 14 and 12 atm, respectively, starting with the side-branch balloon. (5) A second RMS was positioned at the proximal rim of the side branch ostium, resulting in minimal protrusion at the carina. Scaffold was deployed with 12 atm. (6) Then kissing dilation was repeated with a 3.50 mm non-compliant balloon into the main branch and the side-branch scaffolds' balloon after its 2–3 mm pullback. Pressures were 18 and 10 atm respectively. (7) Finally, POT was repeated with a 4.00 mm non-compliant balloon, inflated to 18 atm.

Test #5: Single string technique – large side branch*:* This technique is a modified version of the conventional culotte technique, where the modification targets the minimization of overlapping stent layers. Considering the art of the modification (i.e. choosing the most proximal cell of the SB scaffold for recross in direction of the MB and so reducing of overlap to minimal) the mechanical forces on the scaffold and its structural deformation are the same, as during conventional culotte technique. The procedure was performed as described in literature [4]. (1) First a RMS scaffold was deployed in the side branch with 12 atm, with careful positioning of its proximal edge at the proximal rim of the ostium, resulting in minimal protrusion into the main branch at the level of the carina. (2) Second, the scaffold was proximally optimized by re-inflation of the scaffold delivery balloon at higher pressures (16 atm) after partial pullback. (3) Next the guidewire is slowly pulled back from the side branch until it falls into the first and only protruding cell, through which it was advanced into the distal main branch. (4) Then the protruding cell was opened up to reasonable size with a 1.25 mm balloon (14 atm). (5) A regular guidewire was advanced into the side branch and kissing dilation was performed with 3.00 mm and 3.00 mm balloons in the main branch (through the protruding cell) and in the side branch with 12 and 6 atm, respectively. (6) A second scaffold was positioned into the main branch and deployed at 12 atm. POT was performed with 4.00 mm non-compliant balloon, 20 atm. (7) Then side branch was wired with regular workhorse guidewire through the most distal cell of the main branch scaffold, facing the

side branch ostium. (8) Next final kissing balloon dilation was performed using 3.50 mm and 3.00 mm balloons in the main branch and in the side branch with 18 and 14 atm, respectively. (9) Finally, POT was repeated with a 4.00 mm non-compliant balloon, inflated to 18 atm.

2.2. Optical coherence tomography

Pullback runs were performed at 1 frame/100 μm resolution, using a Dragonfly Duo OCT catheter (St Jude Medical Inc., St. Paul, Minnesota, US) and analyzed by a dedicated workstation (C7-XRTM OCT Intravascular Imaging System, St Jude Medical Inc., St. Paul, Minnesota, US). OCT imaging was done systematically at the end of each procedure for the evaluation of scaffold strut malapposition. For double-scaffold bifurcation procedures OCT was performed in both the main branch and the side branch. Note that OCT imaging was purely documentary and not meant to guide PCI, accordingly it was analyzed off-line and was not reacted by any intervention.

Qualitative OCT analysis was performed based on automated 3-dimensional reconstruction, aiming to identify presence or absence of strut fracture for all cases. For bifurcation cases presence or absence of ostial strut protrusion was evaluated and length of maximal side branch opening was measured.

Quantitative OCT analysis was performed as follows: OCT images were analyzed in the main branch proximal to the side branch ostial area (every fifth frame in 2.5 mm), in the entire side branch ostial area (every third frame; divided into proximal area and carinal area) and distal to the side branch (every fifth frame in 2.5 mm). For double-scaffold bifurcation procedures OCT images were analyzed in the proximal side branch, as well (every third frame in the proximal 2.0 mm).

Malapposition of scaffold struts was calculated as described previously [5] and it was graded as (1) full apposition (no malapposition can be observed) (2) any malapposition (malapposition >0 μm), (3) marked malapposition (malapposition >100 μm).

2.3. Micro computed tomography

μCT imaging (SkyScan 1172 (Bruker, Kontich, Belgium)) was performed in all cases. Quantitative analysis was performed for all the bifurcation cases (#1–#5). Scaffold deformations were visualized at a resolution of 12 μm/voxel. From the scanned volumes the scaffolds were reconstructed by segmentation. Qualitative analysis was based on 3-dimensional reconstruction aiming to identify presence or absence of strut fracture for all cases. Oval deformation and caliber fluctuation was evaluated at several levels, as described in Fig. 1.

3. Results

All in vitro procedures were successfully performed according to the protocol, as described above. No unexpected difficulty was described at any of the procedures. RMSs were advanced easily to main branch and to side branches, when indicated. No unexpected difficulty was described during crossing to the jailed side branch with guide wire or balloon. Subjectively the in vitro performance of the RMSs was comparable to experiences with conventional permanent metallic stents.

3.1. Bifurcations (n = 14)

3.1.1. Test #1 – Main branch scaffolding with side branch opening alone – small side branch (n = 3)

3.1.1.1. Optical coherence tomography. All together 638 scaffold struts were analyzed in 60 OCT frames. In the reconstructed 3-dimensional evaluation, one strut was observed in each case, crossing the side branch orifice, resulting in a maximal length of 'strut-free' side branch orifice of 2.1 mm, 1.5 mm and 2.1 mm, respectively. Overall perfect apposition rates were 93.8%, 91.8% and 95.2% over the three cases. Marked malapposition was observed in 3.8%, 3.7% and 3.8%, respectively, occurring predominantly in the carinal area (79.2% of all markedly malapposed struts). 3-dimensional reconstructed OCT analysis did not reveal any strut fracture.

3.1.1.2. Micro computed tomography. Visual evaluation showed slight opening of the side-branch access without any evidence of overstretched, markedly deformed or fractured struts, as shown in the example case in Fig. 2. Quantitative measurements are detailed in Table 1.

3.1.2. Test #2 – Main branch scaffolding with final kissing dilation – small side branch (n = 3)

3.1.2.1. Optical coherence tomography. All together 571 scaffold struts were analyzed in 60 OCT frames. In the reconstructed 3-dimensional evaluation no crossing-strut facing the side branch orifice was observed in any of the three cases. Accordingly the maximal length of 'strut-free' side branch opening was 1.9 mm, 2.3 mm and 1.8 mm, respectively. Overall perfect apposition rates were 98.4%, 99.0% and 96.7% over the three cases. Marked malapposition was observed in 0.0%, 0.0% and 2.7%, respectively, occurring only in the carinal area (100.0% of all markedly malapposed struts). 3-dimensional reconstructed OCT analysis did not reveal any strut fracture.

3.1.2.2. Micro computed tomography. Visual evaluation showed the improved opening of the side-branch access with scaffolding of the side-

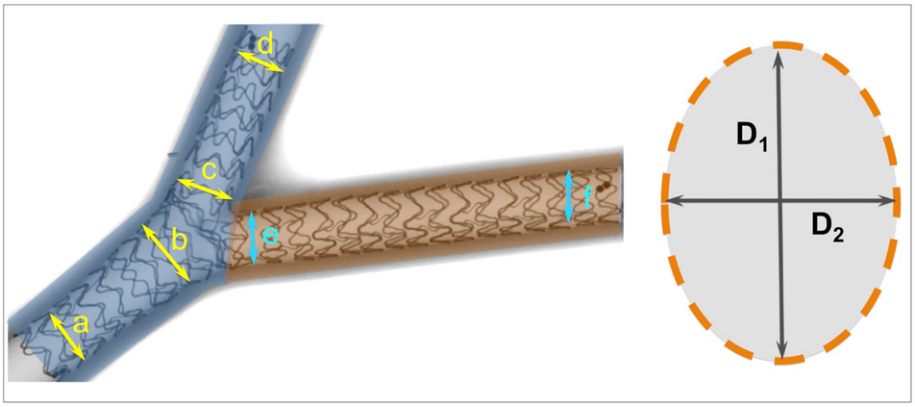

Fig. 1. μCT measurements in bifurcation models. For bifurcation cases oval deformation and caliber fluctuation were evaluated at several levels, namely (a) proximal main branch; (b) proximal main branch at bifurcation; (c) ostial distal main branch; (d) distal main branch; (e) ostial side branch; and (f) distal side branch. D_1 and D_2 indicate largest and smallest diameters, measured only at proximal main branch at bifurcation (b).

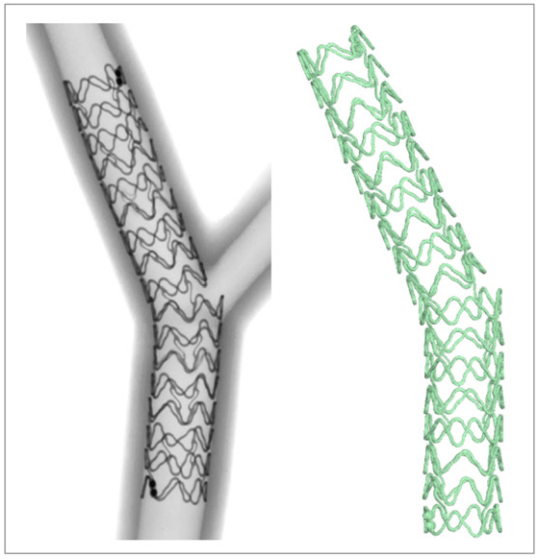

Fig. 2. Bench setting for bifurcation PCI: Main branch scaffolding with side branch opening alone – small side branch. Fluoroscopy (left) and 3D-reconstructed μCT image (right) for visual evaluation of RMSs' performance.

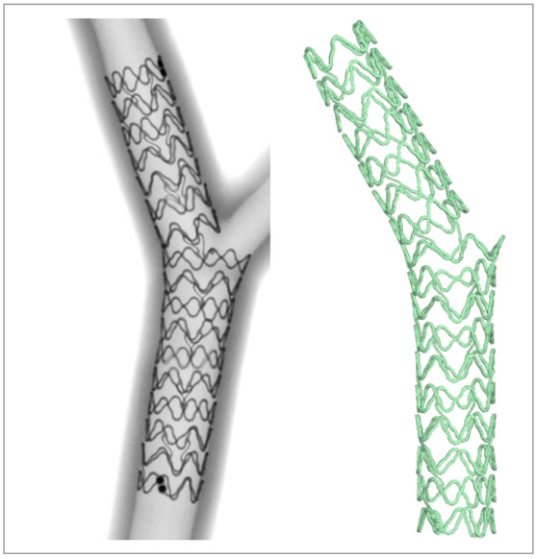

Fig. 3. Bench setting for bifurcation PCI: Main branch scaffolding and final kissing dilation – small side branch. Fluoroscopy (left) and 3D-reconstructed μCT image (right) for visual evaluation of RMSs' performance.

branch ostium, as well. No evidence of overstretched, markedly deformed or fractured struts was observed, see example case in Fig. 3. Measurements are detailed in Table 1.

3.1.3. Test #3 – Main branch scaffolding with final kissing dilation – large side branch (n = 3)

3.1.3.1. Optical coherence tomography. All together 608 scaffold struts were analyzed in 78 OCT frames. In the reconstructed 3-dimensional evaluation no strut was crossing the side branch orifice in any of the three cases. Maximal length of 'strut-free' side branch opening was 3.0 mm, 3.4 mm and 3.1 mm, respectively. Overall perfect apposition rates were 96.1%, 96.2% and 97.7% over the three cases. Marked malapposition was observed in 1.5%, 2.2% and 0.0%, respectively, occurring predominantly in the carinal area (71.4% of all markedly malapposed struts). 3-dimensional reconstructed OCT analysis did not reveal any strut fracture.

3.1.3.2. Micro computed tomography. Visual evaluation showed the massive opening of the side-branch access. In the proximal main branch, at the level of overlapping kissing balloons, struts are markedly straightened, suggestive of being close to the limit of overstretching. However no broken struts were evident, as illustrated in the example case in Fig. 4. Measurements are detailed in Table 1.

3.1.4. Test #4 – T- and protrusion technique (n = 3)

3.1.4.1. Optical coherence tomography. All together 799 scaffold struts were analyzed in 99 OCT frames. According to the reconstructed 3-dimensional evaluation, a strut from the side branch scaffold was crossing the orifice in two cases. The third case was free of 'floating struts'. Maximal length of 'strut-free' side branch opening was 3.3 mm, 3.7 mm and 3.4 mm, respectively. Overall perfect apposition rates were 93.3%, 91.7% and 98.4% over the three cases. Marked malapposition was observed in 5.1%, 4.5% and 1.2%, respectively, occurring dominantly in the carinal area (82.8% of all markedly malapposed struts). 3-dimensional reconstructed OCT analysis did not reveal any strut fracture.

3.1.4.2. Micro computed tomography. μCT demonstrated that the procedure was performed properly with good structural result, as shown on the example case depicted in Fig. 5. Visual evaluation showed the

Table 1
Summary of μCT measurements. Diameter measurements are indicated in in millimeter, according to different locations (a-f), as described in Fig. 1. Single asterisk indicates the bifurcation case with connector fracture. Double asterisk indicates the bifurcation case with strut fracture.

	Main branch					Side branch	
	(a)	(b)		(c)	(d)	(e)	(f)
		$D_{max.}$	$D_{min.}$				
Main branch scaffolding with side branch opening #1	3.09	3.46	3.06	3.04	2.92	–	–
Main branch scaffolding with side branch opening #2	3.14	3.45	3.15	3.12	2.82	–	–
Main branch scaffolding with side branch opening #3	3.15	3.49	2.99	3.04	2.87	–	–
Main branch scaffolding with side branch opening #1 - small	3.10	3.75	3.07	3.00	2.91	–	–
Main branch scaffolding with side branch opening #2 - small	3.16	3.75	3.27	3.07	2.91	–	–
Main branch scaffolding with side branch opening #3 - small	3.06	3.72	3.18	3.08	3.03	–	–
Main branch scaffolding with side branch opening #1 - large	3.65	4.88	3.78	3.15	2.94	–	–
Main branch scaffolding with side branch opening #2 - large	3.65	5.07	3.99	3.62	2.94	–	–
Main branch scaffolding with side branch opening #3 - large	3.65	4.82	4.02	3.34	2.94	–	–
T-and-Protrusion #1 - large	3.36	5.24	3.90	3.47	2.98	3.16	3.04
T-and-Protrusion #2 - large	3.52	5.43	4.11	3.53	2.94	3.55	3.01
T-and-Protrusion #3 - large*	3.44	5.18	4.00	3.59	2.90	3.29	3.10
Single string #1 - large**	3.56	4.50	3.61	3.41	3.09	2.97	3.10
Single string #2 - large	3.51	4.93	3.59	3.31	2.92	3.15	2.95

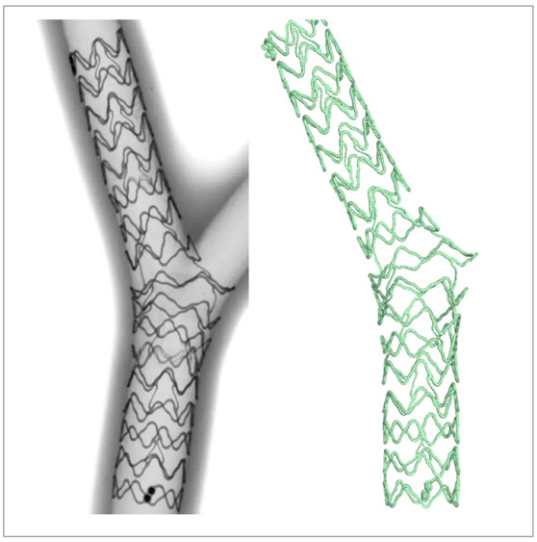

Fig. 4. Bench setting for bifurcation PCI: Main branch scaffolding and final kissing dilation – large side branch. Fluoroscopy (left) and 3D-reconstructed μCT image (right) for visual evaluation of RMSs' performance.

massive opening of the side-branch access and proper scaffolding of the entire bifurcation region. In the proximal main branch, at the level of overlapping kissing balloons, struts are markedly straightened, suggesting that limit of overstretching may have been reached at this level. In one out of the three cases a connector was found broken (Fig. 6A). Note, fracture of connector does not result in loss of radial force. Measurements are detailed in Table 1.

3.1.5. Test #5 – Single string technique (n = 2)

3.1.5.1. Optical coherence tomography. One single string was successfully crossed in both cases. All together 564 scaffold struts were analyzed in 66 OCT frames. Maximal length of 'strut-free' side branch opening was 3.8 mm and 5.1 mm, respectively. Overall perfect apposition rates were 92.2% and 98.9% over the two cases. Marked malapposition was observed in 0.7% and 0.4%, respectively, occurring in 66.7% in the carinal area. 3-dimensional reconstructed OCT analysis was not feasible due to technical limitations.

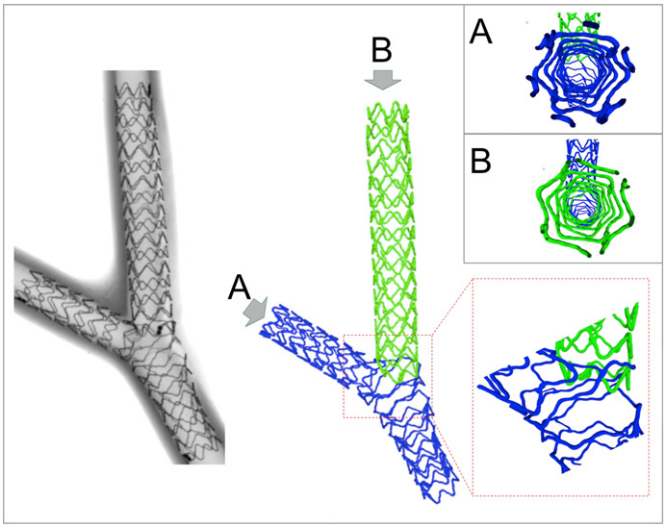

Fig. 5. Bench setting for bifurcation PCI: T-and-Protrusion technique – large side branch. Fluoroscopy (left) and 3D-reconstructed μCT image (right) for visual evaluation of RMSs' performance. A and B panels indicate longitudinal luminal views from distal main branch and distal side branch, respectively.

3.1.5.2. Micro computed tomography. μCT demonstrated that the procedure was performed properly with good structural result, as shown on the example case in Fig. 7. Visual evaluation showed the massive overstretching of the 'single string', which resulted in strut fracture in one of the two cases (Fig. 6B). Measurements are detailed in Table 1.

4. Discussion

The introduction of bioresorbable scaffolds aims to revolutionize PCI. The vision is to offer proper scaffolding in the early post-PCI phase and 'un-caging' of the vessel in the long term, allowing restoration of normal vessel wall structure and recovery of physiologic vasomotion. Even though this is a major advantage, the trade-off is that structural and mechanical characteristics of these devices are different to conventional metallic stents: struts are thicker, less expandable and more fragile [6,7]. Therefore what is still appropriate practice with conventional metallic stents, the same might be inappropriate handling for resorbable scaffold, resulting in underexpansion, malapposition, strut fracture and acute recoil or even strut embolization. And as outcome, it can be associated with major clinical consequences, such as restenosis or stent thrombosis. The latter has been well demonstrated during the early era of first generation poly-L-lactic acid bioresorbable scaffolds, when various complex interventions, such as calcified lesions, tortuous vessels and complex bifurcations have been attempted, resulting in significantly higher adverse event rates compared to the same cases treated with conventional metallic stents [8–11].

Accordingly, knowing and understanding the technical characteristics of these devices is the cornerstone of correct interventional practices and vital in order to avoid potential complications. First of all, this includes proper lesion selection, namely lesions in vessels where a restoration of normal endothelial function can be expected. Second the proper sizing, meaning that scaffold integrity should not be jeopardized by exceeding expansion capacity. On this aspect, magnesium might be more forgiving than the original poly-L-lactic acid used to be. The latter is especially important in the case of bifurcations where the fractal geometry indicates two different diameters with a well defined step-down between proximal and distal main branch segments. Finally, considering the lower radial strength of RMS proper lesion preparation is crucial, as well as the adequate scaffold postdilation [12].

In this study we investigated the in vitro performance of the latest generation RMS in bifurcations, treated with (1) POT-side branch-POT fashion; (2–3) provisional T-stenting with final kissing dilation of small or large side branches; (4) T-and-Protrusion double stent technique or with (5) single string double stent technique, which is a slight modification of the conventional culotte technique approaching minimization of double layer.

All in vitro procedures were performed successfully with good final result according to fluoroscopic guidance. Final results were evaluated by OCT and μCT. OCT demonstrated proper strut apposition, while malapposition occurred mainly in bifurcation cases, predominantly in the carinal area, as expected. Considering that previous in vitro and in vivo studies, with limited sample sizes using mainly conventional metallic stents, investigating various bifurcation techniques reported malapposition rates in the region of bifurcation ranging between 30 and 45%, present data can be considered at least comparable, if not favorable [4,13–14]. No relevant malapposition was seen at the proximal main branch confirming the proper conformability of the RMS, at least in the indicated range of diameters. No strut fractures or major deformations were revealed by OCT. Even though a direct comparison with any conventional metallic device was not performed in the present study, the observed performance is comparable with previous in vitro and in vivo data with conventional metallic stents [4,13–14]. This finding is also aligned with the limited animal data using RMS in bifurcations [15].

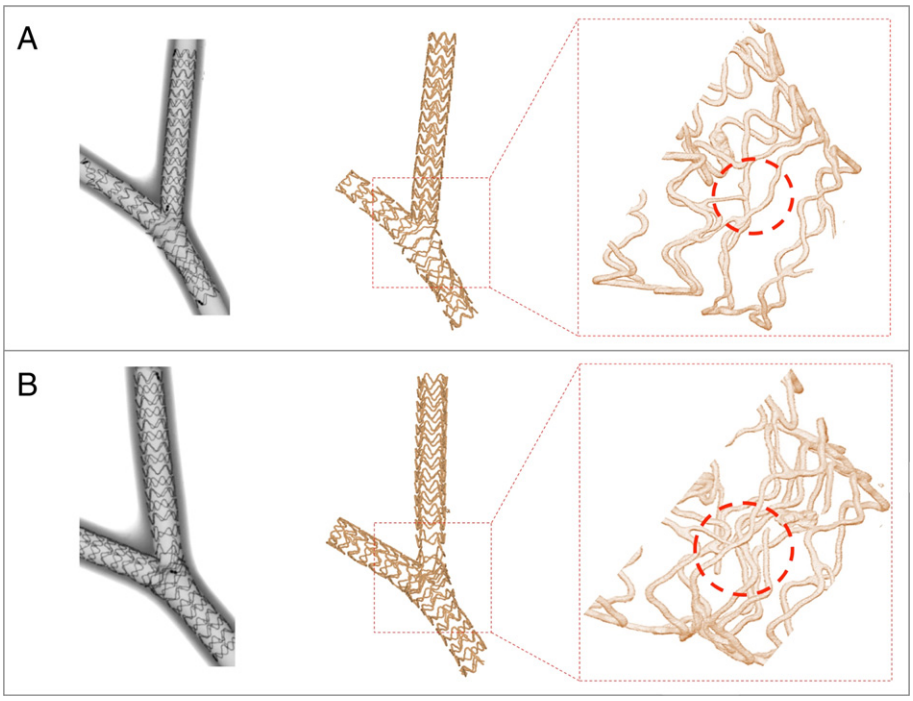

Fig. 6. Scaffold fractures. Fluoroscopy (left) and 3D-reconstructed μCT images (right) of a T-and-Protrusion case (A) and a Single string technique case (B), where careful μCT analysis identified a connector fracture and a strut fracture, respectively.

μCT analysis has mainly confirmed these findings, however where the main branch stents are proximally massively postdilated with final kissing dilation, the struts are almost fully stretched. Accordingly in one case a broken connector (T and protrusion technique) and in another case, a broken strut (String technique) were identified. Note that the spots were not identifiable by OCT, not even after using μCT images for guidance. The latter raises the question, how often it might occur and be overseen in experimental in vivo studies or even in daily clinical practice. Still, it is crucial to realize that overexpanding the struts of RMS is indeed an issue with potential structural complications and potential adverse clinical consequences. Accordingly, avoidance of overexpansion is of critical importance. Therefore, considering potential use in bifurcations, not only 'luminal expansion capacity' but also 'side-cell expansion capacity' should be clearly reported, whenever a new scaffold with fragile struts is introduced.

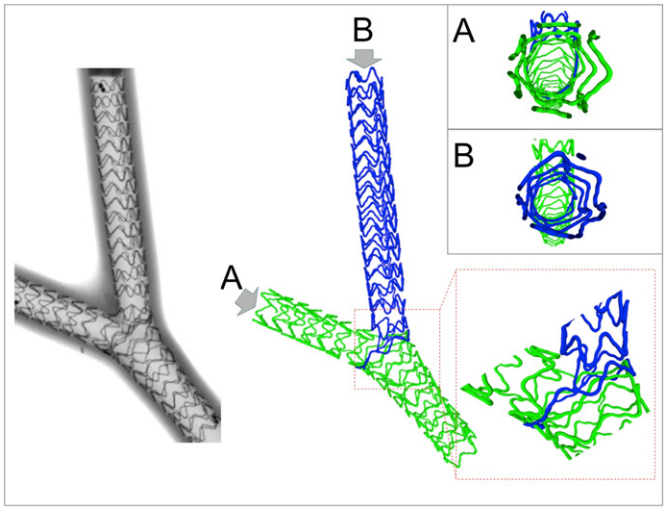

Fig. 7. Bench setting for bifurcation PCI: Single string technique – large side branch. Fluoroscopy (left) and 3D-reconstructed μCT image (right) for visual evaluation of RMSs' performance. A and B panels indicate longitudinal luminal views from distal main branch and distal side branch, respectively.

The study has limitations to be acknowledged. First of all, sample size is low, requiring very careful interpretation. Still, results can be used for further orientation of future investigations. Second, acute structural performance was not directly compared either with any currently available latest generation metallic stents or with any other resorbable scaffolds. Performance of the RMS is compared purely with data from the literature and therefore somewhat speculative. Third, being purely an in vitro evaluation, there are several conditions (i.e. role of plaque composition, presence of calcification, additional bends, etc.), which were not applicable and therefore linking our findings directly to potential clinical outcomes is speculative at this stage and requires further clinical investigation. But despite these limitations, we believe the results demonstrate key learning points about the use of RMSs and might serve to inform future clinical investigations. Of note, until further clinical testing becomes available, performing complex bifurcation PCI with RMS is still strongly discouraged [12,16].

5. Conclusion

Current generation resorbable magnesium scaffolds can structurally cope with bifurcations in various in vitro models. Still, for cases (i.e. large diameter step down, large side branches, etc.) and techniques (culotte, string, etc.) where massive overexpansion of the scaffold (i.e. the lumen or any cell) is needed, RMS might not be the proper device due to a definite risk of strut fracture. This investigation may justify future clinical evaluation of the device in complex coronary anatomies using standardized procedural techniques [2].

Perspectives

What is known: Resorbable devices are different to conventional metallic stents: struts are thicker, less expandable and more fragile. Therefore what is still appropriate practice with conventional metallic stents, the same might be inappropriate for resorbable scaffold, resulting potentially in underexpansion, malapposition, strut fracture and acute recoil or

even strut embolization. These might be, of course associated with major clinical consequences, such as restenosis or stent thrombosis.

What is new: Latest generation resorbable magnesium scaffolds can structurally cope with bifurcations in various in vitro models, where no massive overexpansion of the scaffold is needed.

What is next: This investigation justifies future clinical evaluation of resorbable magnesium scaffold in complex coronary anatomies such as bifurcations, using standardized procedural techniques.

Acknowledgment

The present study did not receive any financial support. The investigated RMSs were provided unrestrictedly by Biotronik AG, free of charge.

References

[1] Lassen JF, Holm NR, Banning A, et al. Percutaneous coronary intervention for coronary bifurcation disease: 11th consensus document from the European Bifurcation Club. EuroIntervention 2016;12:38–46.
[2] Milasinovic D, Wijns W, Ntsekhe M, Hellig F, Mohamed A, Stankovic G. Step-by-step manual for planning and performing bifurcation PCI: a resource-tailored approach. EuroIntervention 2018;13:e1804–11.
[3] Burzotta F, Gwon HC, Hahn JY, et al. Modified T-stenting with intentional protrusion of the side-branch stent within the main vessel stent to ensure ostial coverage and facilitate final kissing balloon: the T-stenting and small protrusion technique (TAP-stenting). Report of bench testing and first clinical Italian-Korean two-centre experience. Catheter Cardiovasc Interv 2007;70:75–82.
[4] Toth GG, Pyxaras S, Mortier P, et al. Single string technique for coronary bifurcation stenting: detailed technical evaluation and feasibility analysis. JACC Cardiovasc Interv 2015;8:949–59.
[5] Lowe HC, Narula J, Fujimoto JG, Jang IK. Intracoronary optical diagnostics: current status, limitations, and potential. J Am Coll Cardiol Intv 2011;4:1257–70.
[6] Foin N, Lee R, Bourantas C, et al. Bioresorbable vascular scaffold radial expansion and conformation compared to a metallic platform: insights from in vitro expansion in a coronary artery lesion model. EuroIntervention 2016;12:834–44.
[7] Foin N, Lee R, Mattesini A, et al. Bioabsorbable vascular scaffold overexpansion: insights from in vitro post-expansion experiments. EuroIntervention 2016;11:1389–99.
[8] Tamburino C, Latib A, van Geuns RJ, et al. Contemporary practice and technical aspects in coronary intervention with bioresorbable scaffolds: a European perspective. EuroIntervention 2015;11:45–52.
[9] Stone GW, Abizaid A, Onuma Y, et al. Effect of technique on outcomes following bioresorbable vascular scaffold implantation: analysis from the ABSORB trials. J Am Coll Cardiol 2017;70:2863–74.
[10] Ali ZA, Gao RF, Kimura T, et al. Three-year outcomes with the absorb bioresorbable scaffold: individual-patient-data meta-analysis from the ABSORB randomized trials. Circulation 2018;137:464–79.
[11] Kereiakes DJ, Ellis SG, Metzger C, et al. 3-year clinical outcomes with everolimus-eluting bioresorbable coronary scaffolds: the ABSORB III trial. J Am Coll Cardiol 2017;70:2852–62.
[12] Fajadet J, Haude M, Joner M, et al. Magmaris preliminary recommendation upon commercial launch: a consensus from the expert panel on 14 April 2016. EuroIntervention 2016;12:828–33.
[13] Tyczynski P, Ferrante G, Moreno-Ambroj C, et al. Simple versus complex approaches to treating coronary bifurcation lesions: direct assessment of stent strut apposition by optical coherence tomography. Rev Esp Cardiol 2010;63:904–14.
[14] Viceconte N, Tyczynski P, Ferrante G, et al. Immediate results of bifurcational stenting assessed with optical coherence tomography. Catheter Cardiovasc Interv 2013;81:519–28.
[15] Bennett J, Vanhaverbeke M, Vanden Driessche N, et al. The drug-eluting resorbable magnesium vascular scaffold in complex coronary bifurcations: insights from an in vivo multimodality imaging study. EuroIntervention 2018;13:2036–46.
[16] Byrne RA, Stefanini GG, Capodanno D, et al. Report of an ESC-EAPCI Task Force on the evaluation and use of bioresorbable scaffolds for percutaneous coronary intervention: executive summary. Eur Heart J 2018;39:1591–601.